Microwave-heated γ-Alumina Applied to the Reduction of Aldehydes to Alcohols

Bhausaheb Dhokale[+],[a] Arturo Susarrey-Arce[+],*[b, c] Anna Pekkari,[a] August Runemark,[a] Kasper Moth-Poulsen,[a] Christoph Langhammer,[b] Hanna Härelind,[d] Michael Busch,[e] Matthias Vandichel,*[f] and Henrik Sundén*[a, g]

The development of cheap and robust heterogeneous catalysts for the Meerwein-Ponndorf-Verley (MPV) reduction is desirable due to the difficulties in product isolation and catalyst recovery associated with the traditional use of homogeneous catalysts for MPV. Herein, we show that microwave heated γ-Al_2O_3 can be used for the reduction of aldehydes to alcohols. The reaction is efficient and has a broad substrates scope (19 entries). The products can be isolated by simple filtration, and the catalyst can be regenerated. With the use of microwave heating, we can direct the heating to the catalyst rather than to the whole reaction medium. Furthermore, DFT was used to study the reaction mechanism, and we can conclude that a dual-site mechanism is operative where the aldehyde and 2-propoxide are situated on two adjacent Al sites during the reduction. Additionally, volcano plots were used to rationalize the reactivity of Al_2O_3 in comparison to other metal oxides.

1. Introduction

Alcohols have a ubiquitous role in nature and can be found in everything from pharmaceuticals to materials. Therefore, the reduction of aldehydes to alcohols is undoubtedly a very important chemical transformation.[1–6] The most common way to reduce an aldehyde to alcohol is to employ a stoichiometric amount of a hydride-based reagent or a transition metal-based catalyst in combination with a hydrogen source. Even though these reactions are highly selective and high yielding, their usage is problematic due to poor atom economy, the scarcity of transition metals, waste disposal, and safety issues.[7,8] These issues can partially be avoided by employing the MPV reduction.[9,10] In the MPV reduction a keto compound is reduced to the corresponding alcohol via a transfer of a hydride from a sacrificial low molecular weight alcohol over a homogeneous Al-based catalyst.[11–16] However, separation of the homogeneous catalyst and purification of the formed alcohol usually requires column chromatography leading to solvent losses and thus providing these reactions with a high E-factor.[17,18] In this perspective, heterogeneous catalysis offers an obvious benefit as most heterogeneous catalyst in principle can be removed from the reaction mixture by a simple filtration and thereby also regenerated.

A number of heterogeneous catalysts have been developed for the MPV reduction,[19] such as, zeolites,[20–25] mesoporous silicates,[26] hydrotalcite,[27,28] metal oxides[29–35] or metal-organic frameworks.[36,37] However, most of them involve complex synthetic routes with the incorporation of various metals[24,25,38,39] and in some cases rare metals.[40] An inexpensive, readily available robust and non-toxic catalyst material for the heterogeneous MPV reduction would be highly desirable.

Alumina (Al_2O_3) meets most of the above-mentioned criteria. However, for the MPV reduction, Al_2O_3 performs poorly, and it is very often doped with other elements to enhance its reactivity.[41–47] In this work, we argue that alumina, with the

[a] Dr. B. Dhokale,[+] A. Pekkari, A. Runemark, Prof. K. Moth-Poulsen, Prof. H. Sundén
Chemistry and Chemical Engineering
Chalmers University of Technology
412 96 Gothenburg (Sweden)
[b] Dr. A. Susarrey-Arce,[+] Prof. C. Langhammer
Department of Physics
Chalmers University of Technology
412 96 Gothenburg (Sweden)
[c] Dr. A. Susarrey-Arce[+]
Mesoscale Chemical Systems
MESA + Institute
University of Twente
P.O. Box 217
Enschede 7500AE (Netherlands)
E-mail: a.susarreyarce@utwente.nl
[d] Prof. H. Härelind
Competence Centre for Catalysis
Department of Chemistry and Chemical Engineering
Chalmers University of Technology
412 96 Gothenburg (Sweden)
[e] Dr. M. Busch
Department of Chemistry and Material Science
School of Chemical Engineering
Aalto Universit
02150 Espoo (Finland)
[f] Dr. M. Vandichel
Department of Chemical Sciences and Bernal Institute
University of Limerick
Limerick V94 T9PX (Ireland)
E-mail: matthias.vandichel@ul.ie
[g] Prof. H. Sundén
Chemistry and Molecular Biology
University of Gothenburg
412 96 Gothenburg (Sweden)
E-mail: sundenh@chalmers.se
henrik.sunden@chem.gu.se
[+] These authors contributed equally

Supporting information for this article is available on the WWW under https://doi.org/10.1002/cctc.202001284

right activation mode, can serve as a good catalyst material due to the occurrence of several coordination sites that are present on the catalyst surface that is set up to coordinate both a carbonyl and alcohol. A suitable activation mode is microwave irradiation. In the literature, there are several reports on microwave-assisted heating of alumina. For instance, sintering of alumina based ceramics can be performed under microwave irradiation leading to materials with substantially different properties as compared to materials made with conventional heating.[48] Furthermore, there are several reports on microwave-assisted alumina mediated reactions[49] such as alkylation[50] and condensation reactions[50–53] or a combination of the two.[54] From these reports, it seemed likely that microwave heating could be used to enhance the catalytic properties of alumina in the MPV reduction through direct heating of the catalyst. The use of microwave radiation to carry out MPV reaction in the presence of activated neutral or basic alumina in a domestic microwave oven was required to use the catalytic amount of bases.[55] Herein, we report a reduction of aldehydes to alcohols over a heterogeneous γ-Al_2O_3 using microwave-assisted heating. The scope of the reduction is broad and includes aromatic, unsaturated and aliphatic aldehydes and is compatible with a high degree of substituents without compromising conversion and selectivity. Mechanistically, contrary to the conventional MPV single site mechanism,[19,56–59] we propose via density functional theory (DFT) the preference for a dual-site mechanism, where 2-propanol forms an 2-propoxide onto a Lewis acid site which subsequently transfers hydrogen to the carbonyl group adsorbed on a neighbouring Lewis acid site. Our computational analysis confirms that among other oxides typically used for MPV, γ-Al_2O_3 is the catalyst of choice for the reduction of aldehydes.

2. Results and Discussions

2.1. MPV reduction

Our study commenced with the evaluation of nine different alcohols as the hydride source under microwave heating conditions (Figure S1.1). The results from this initial screening showed that secondary alcohols like 2-propanol were superior for the reduction of cinnamaldehyde providing the cinnamyl alcohol in 99% conversion and selectivity. Hence, 2-propanol was selected as the sacrificial reducing agent. To evaluate the effects of microwave heating, the reaction was performed using a conventional heating block at 180 °C and the reaction outcome was followed using gas chromatography (Figure S1.9). A fourth-fold decrease in reaction rate compared to microwave heating was observed. The significant difference in reaction outcome points towards that microwave heating is a key element in the γ-Al_2O_3 catalyzed MPV reduction of aldehydes. A viable explanation is that the microwave heating ensures rapid and homogeneous heating of the reaction mixture,[60] [61] but also provides direct heating of the catalyst which can efficiently promote a faster reaction on the γ-Al_2O_3 surface. In contrast, conventional heating heats the reaction vessel from the outside to the inside, resulting in a slower heating, something that is reflected in the lower reaction rate.[60,62–65]

Poor chemoselectivity is a common issue for the reduction of α,β-unsaturated carbonyl compounds with metal hydrides. Hence, the scope of the optimized MW heating reaction was investigated utilizing a series of α,β-unsaturated aldehydes. As it turns out, α,β-unsaturated aldehydes perform well delivering a broad range of allylic alcohols in excellent yields and chemoselectivity (Figure 1). The reaction shows high functional group compatibility and functional groups such as nitro, and halogens (fluoro, chloro) and methoxy are well tolerated providing the corresponding allylic alcohols in 95–98% yield, with high chemoselectivity (entries **2b**–**2f**). Next, benzaldehydes were investigated as reaction partners in the heterogeneous MPV reduction. Both electron-rich and electron-deficient aldehydes are well tolerated, and the corresponding benzylic alcohols could be isolated in almost quantitative yields (entries **2g**–**2m**). Furthermore, the heteroaromatics furfural and 3- and 4-pyridinecarboxaldehyde can also be reduced to their alcohol counterparts in 92%, 98%, and 95% yield, respectively (entries **2n**–**2p**). It is worth noting that the valorization of furfural (**1n**) to furfuryl alcohol (**2n**) is a synthetically important transformation in the production of valuable chemicals and biofuel. Table S3 (ESI) compares the selected efforts devoted to carrying out this transformation. We are reporting this transformation without expensive novel and non-novel metals catalyst, without H_2 gas, and without the column chromatographic purification with an isolated yield of 92%.[66–69] Reduction of a non-activated aldehyde was also possible with 3-phenyl propanal reduced to 3-phenylpropanol with an isolated yield of 78% (entry **2q**). Finally, sterically demanding α,β-unsaturated aldehydes with substituents in the α-position can be reduced affording the α-amylcinnamyl alcohol and α-bromocinnamyl alcohol both in 97% yield (entries **2r** and **2s**). To reach full conversion, α-amylcinnamaldehyde and the α-bromocinnamaldehyde required twice the amount of γ-Al_2O_3, *i.e.*, 200 mg. The higher loading needed for these two entries is ascribed to the bulky substituents in the α-position, thus making them less reactive. From these results, it is clear that selective reduction of α,β-unsaturated carbonyl and other aldehydes with 2-propanol can be achieved over γ-Al_2O_3 with microwave heating.

In the reaction scope, it was also observed that aldehydes bearing aromatic substituents such as tertiary amines and hydroxyls generate ethers rather than alcohols (Figure 2). For example, dimethylamino substituted aldehydes generated the corresponding ethers as the only product with 94% and 90% yield, respectively (entries **3t** and **3u**). Similarly, hydroxy-substituted aldehydes also yielded ethers (entries **3v** and **3w**) that could be isolated in 60% and 62% yield. In an effort to shed some light on the etherification mechanism we performed two reactions starting from vanillyl alcohol. Vanillyl alcohol was microwave heated in the absence of γ-Al_2O_3. Under these conditions, no ether is formed indicating that the γ-Al_2O_3 is active in the etherification step (Figure 3a). This notion was further supported by an experiment where vanillyl alcohol in the presence of γ-Al_2O_3, under standard conditions, reacts to

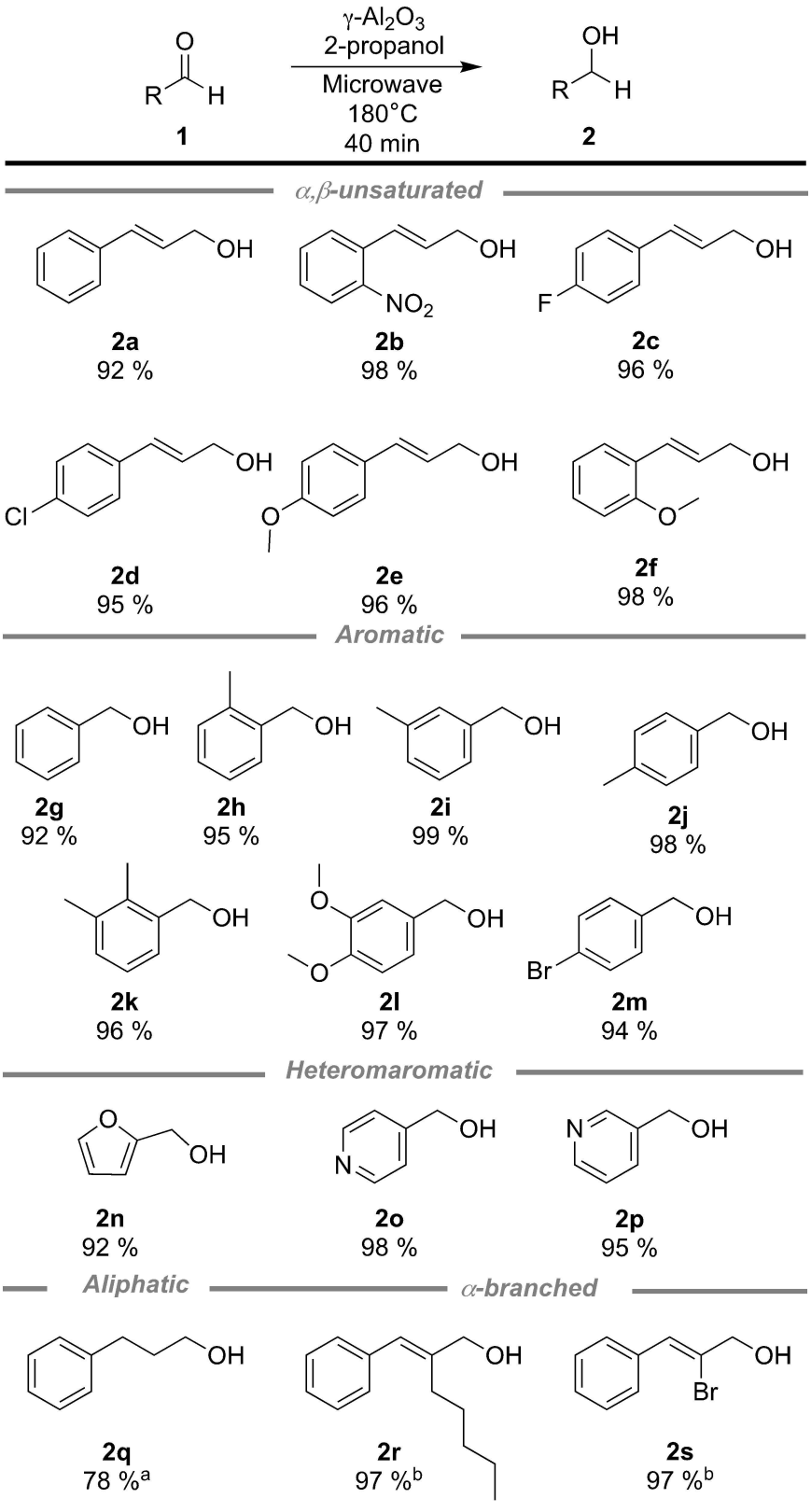

Figure 1. Scope of reaction methodology for different aldehydes. All yields are reported after filtration of reaction mixture and evaporation of the solvent. [a] Isolated by column chromatography (reactant purity 90%). [b] 200 mg of catalyst used.

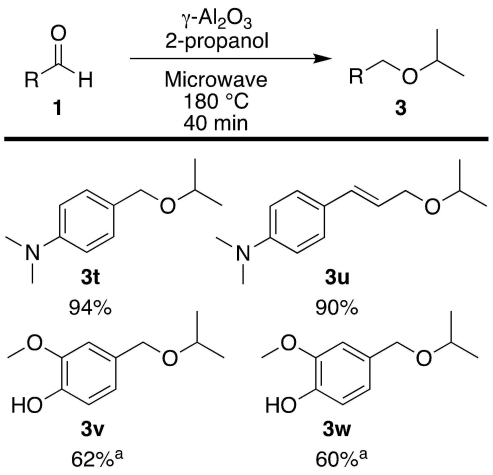

Figure 2. Scope of reaction for amine and phenol substituted aldehydes. All yields are reported after filtration of reaction mixture and evaporation of the solvent. [a] Isolated by column chromatography.

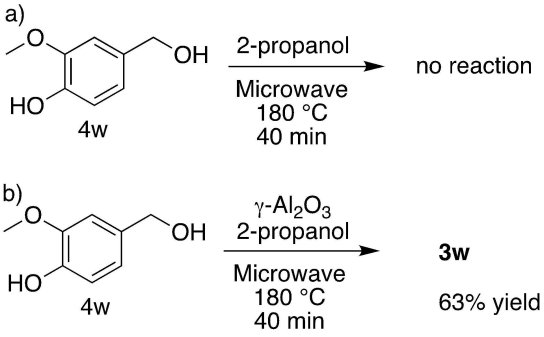

Figure 3. Etherification reaction of vanillyl alcohol. a) standard reaction conditions without γ-Al_2O_3. b) Standard conditions with γ-Al_2O_3.

form the isopropyl ether (Figure 3b). From these results we propose a reaction mechanism for the etherification where the aldehyde is first reduced to the allylic alcohol in accordance with the MPV mechanism. Next, the alcohol is deoxygenated by the aid of the alumina to render a *p*-quinone methide that reacts with isopropanol to form the isopropyl ether.

2.2. Catalyst reusability performance and thermal treatment

After having evaluated the scope of the heterogenous MPV reduction and shown that the reaction is high yielding, chemoselective, and requires only filtration to separate the catalyst from the pure product, our attention turned towards the reusability of the catalyst. For the first set of reusability experiment, we used the same γ-Al_2O_3 in four consecutive MPV reduction cycles (*i.e.*, starting with fresh γ-Al_2O_3 and reusing it three times, data shown in Figure 4a). It is found that the cinnamaldehyde conversion steadily decreases from 100 to 30% over three reaction periods. However, irrespective of the conversion-loss, the selectivity is maintained at 80% or higher for the fresh, 1st cycle, and 2nd cycle followed by a 40% drop in

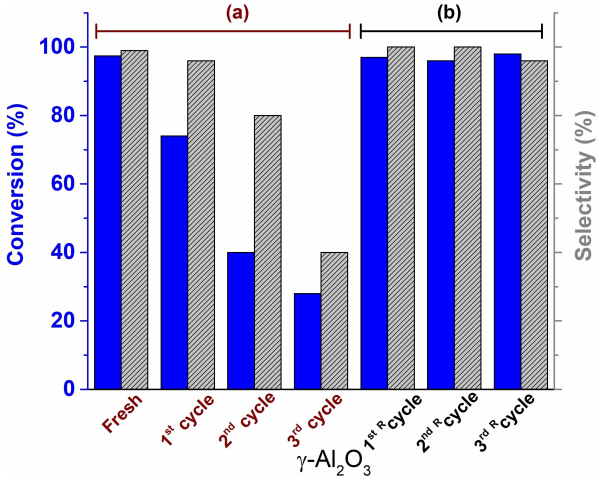

Figure 4. a) Conversion and selectivity as a function of the recyclability cycle for the fresh, 1st cycle, 2nd cycle, and 3rd cycle. b) Conversion and selectivity for three recovery cycles 1st cycle (1st Rcycle), 2nd (2nd Rcycle), and 3rd cycle (3rd R cycle).

the 3rd cycle. The conversion-loss may be explained by increased inaccessibility of the aluminium oxide surface due to coke formation *i.e.* accumulation of carbon[70] or water or structural changes of the solid phase. Therefore, the fresh and 1st cycle used γ-Al_2O_3 were analyzed with X-ray photoemission spectroscopy (XPS) to generate understanding of conversion-losses due to the carbon accumulation. The results show that the carbon content over the γ-Al_2O_3 increased after the 1st reaction cycle (Figure S1.3) suggesting the presence of carbon deposits blocking Al sites, thus decreasing the catalytic activity for the 1st cycle and subsequent 2nd cycle. Next, we looked at the effect of water content. These experiments were made to investigate water poisoning and reveal that water content is deleterious for the activity of the catalyst (Figure S1.4). The effect is clear and can be seen already in the presence of 1% of water with the reaction stopping at 50% conversion. To this end, the potential structural changes of the γ-Al_2O_3 were investigated with x-ray diffraction (XRD) (Figure S1.5).[71] No structural differences can be seen between the fresh and the 1st cycle and 3rd cycle. Taken together, the results suggest that catalyst deactivation is due to the accumulation of carbon and/or water adsorption in the catalyst after the reaction, blocking the active acid sites on γ-Al_2O_3. Thermal treatment over the catalyst was performed to remove the blocking acid sites from residues during reusability from the γ-Al_2O_3. It is clear that with this treatment, the catalyst recovers (R) with the γ-Al_2O_3 nominally regaining its activity. The results indicate that the catalyst can be used in the MPV reduction of cinnamaldehyde as confirmed with the increase of conversion and selectivity (^{R}cycle in Figure 4b). It is important to note that the objective of this thermal treatment is not to study the catalyst deactivation mechanism nor targeted as a recycling experiment. However, it could generate insights into the potential use of thermal treatment to remove adsorbed species over the catalyst after each MPV reduction reaction cycle.

2.3. Acid sites in γ-Al_2O_3

Next, we utilized pyridine (Py) as a molecular probe to identify the type of acid sites in γ-Al_2O_3. The Py IR spectra for a pre-treated γ-Al_2O_3 at 200 °C samples is shown in Figure 5a. The three IR bands located at 1450, 1492 and 1615 cm^{-1} are assigned to Py-adsorbed on a Lewis acid center[72,73] (*e.g.*, Al-site). No characteristic IR bands for Brønsted acid sites (~ 1540 cm^{-1}) are found. This can be attributed to the low surface concentration of Brønsted sites in γ-Al_2O_3. To probe weak Brønsted acid sites we adsorbed 2,6-lutidine (Lu) over a similarly pre-treated γ-Al_2O_3. The reason for utilizing Lu is because of its weak affinity to Lewis acid sites (i. e. steric hindrance induced by the methyl groups).[74] The IR spectra for the adsorbed Lu over the pre-treated catalyst is displayed in Figure 5b. No Lu-peak around 1630–1650 cm^{-1} was recorded indicating the absence or low amount of Brønsted acids.[74,75] The broad IR band around 1456 cm^{-1} in Figure 5b is assigned to Lewis acid sites.[75] From our results, it is clear that the main active sites available for aldehyde reduction reactions are the Lewis acid sites. The results on IR-probed acid sites are in good agreement with the total acidity of γ-Al_2O_3 (*i.e.*, 1.02 μmol m^{-2}) derived from the ratio of total acidity obtained with temperature-programmed desorption of NH_3 and surface area measurements in Table S2.

2.4. Mechanistic insights on γ-Al_2O_3

The reduction of cinnamaldehyde to cinnamyl alcohol was chosen as our model reaction owing to the possibility of reduction of both the carbon-carbon double bond and the carbonyl group present. The level of complexity of the experimental system and the limitations imposed by DFT are significant. Several simplifications need to be made when modelling the reaction and constructing the model system. Using this ansatz, it is not possible to include microwave heating effects other than selective heating of the solid phase. Including MW-heating would require detailed knowledge of the interface between water and the oxide, which is still unknown.[76] The difference between traditional thermal heating and microwave heating is that MW-radiation increases the rotational entropy of H_2O molecules, while thermal heating more directly affects vibrational entropy.[60] Furthermore, the deprotonation and protonation steps of the alcohols are omitted. This is justified as these steps are usually fast and typically only require to overcome a negligible activation barrier.[77–81] Instead, we focused on the mechanistic aspects of the heterogeneous γ-Al_2O_3 catalysed MPV-reduction. Hence, the reaction mechanism of the MPV reaction is studied using a γ-Al_2O_3 (110) model system where 1 additional water molecule is kept within the unit cell. This corresponds to an OH coverage of 3 OH groups per nm^2 (see Figure S1.2). The reason to keep this chemisorbed water molecule lies in the very high energy gain of more than −200 kJ/mol for the first dissociative chemisorption on the bare γ-Al_2O_3 (110) model system. Therefore, this type of chemisorbed water is even very hard to remove in vacuum conditions at high temperature (Figure S1.2). Note that our simplified model excludes the presence of defects, like edges, kinks, or steps in the γ-Al_2O_3.

Building on these simplifications and using the above-described model system, it is now possible to study the reaction mechanism. The MPV reaction may in principle proceed through a single- or dual-site mechanism (Figure 6a). Both routes possess an equivalent reaction sequence but differ by assuming the adsorption of the reactants at a single Al site (a single-site mechanism) or the adsorption at two adjacent Al sites (a dual-site mechanism). In both mechanisms, the reaction is initialized by the adsorption of isopropanol (R→A). Assuming a low coverage (LC) situation where apart from the dissociated water molecules, no other adsorbates are present, this reaction is exergonic by −125 kJ/mol (State A, Figure 6b) for either reaction route. At higher 2-propoxide coverage (HC), we have considered chemisorbed 2- propoxide on two different active sites in our model system, site *1 and *2 (see Figure S1.6). These

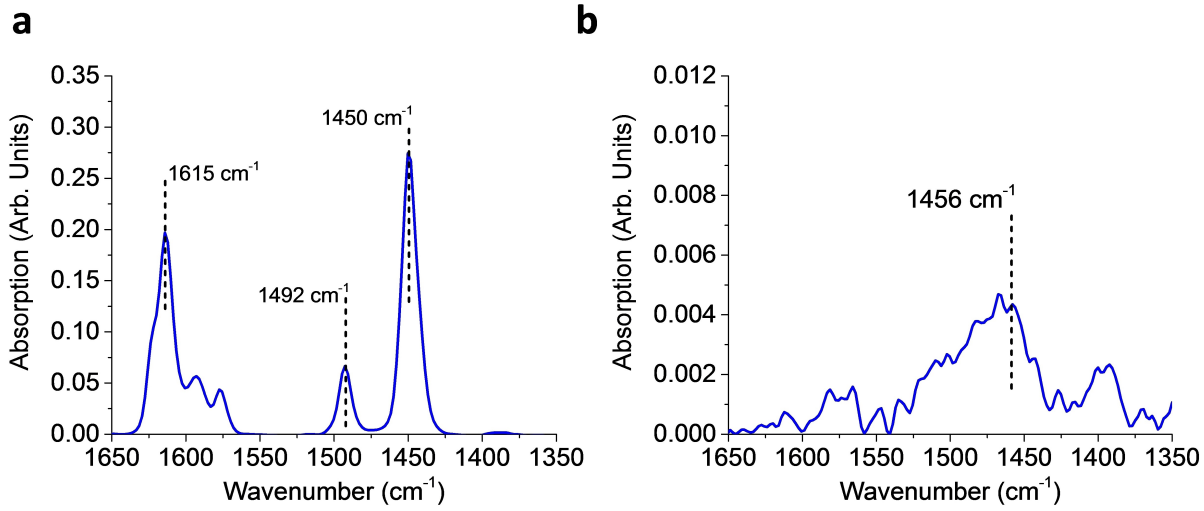

Figure 5. IR spectra for adsorbed a) pyridine and b) 2,6-lutidin over γ-Al_2O_3 catalyst.

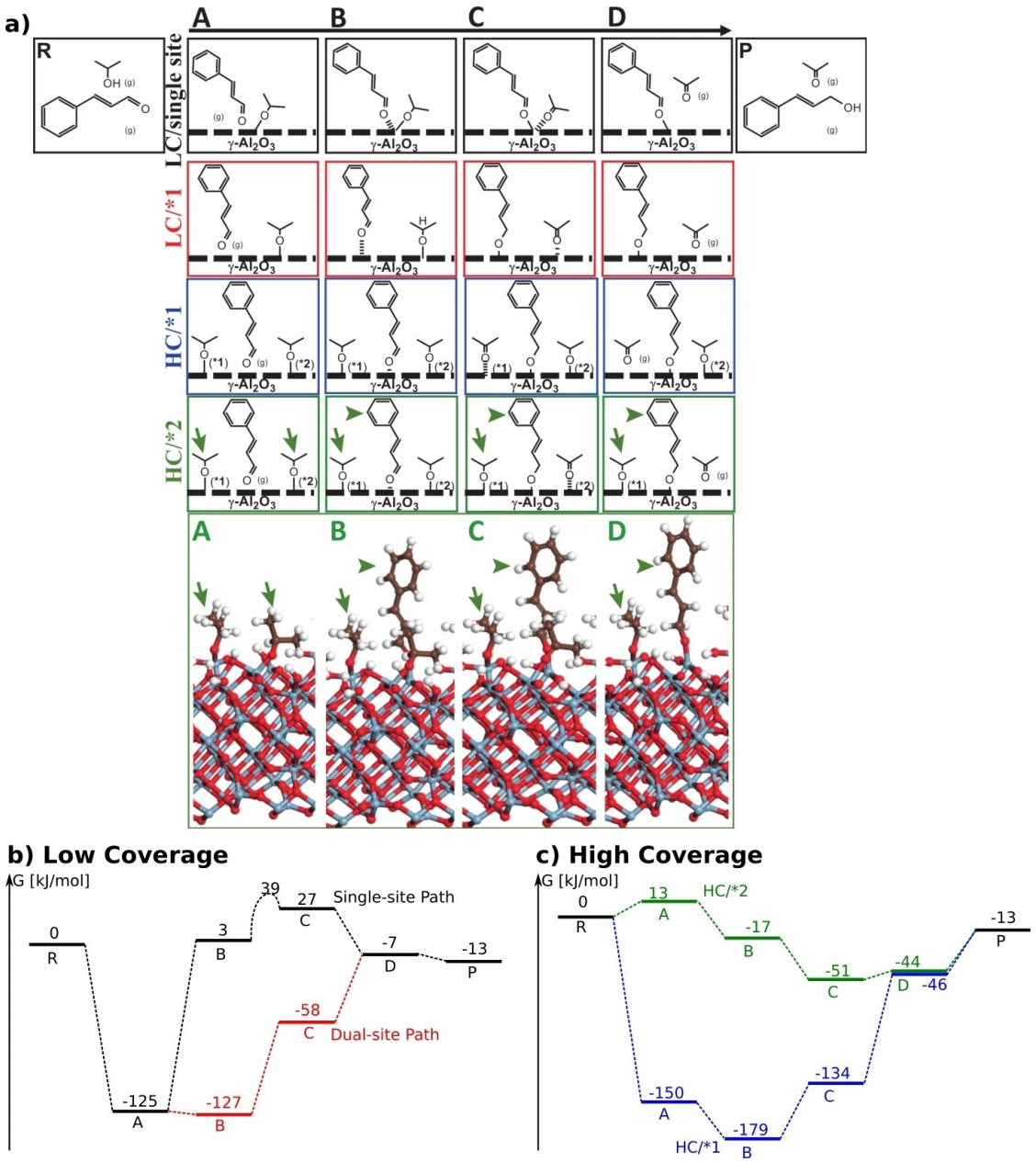

Figure 6. a) Schematic representation of the single site (LC/single Site) and dual-site (LC/*1) mechanisms at low (LC) and high (HC) 2-propanol coverage. Atomic colour codes: aluminium (light grey), oxygen (red), carbon (brown), hydrogen (white). b) Free energy diagram for the single and dual-site paths at low coverage. c) Free energy diagram of the dual-site mechanism at high 2-propanol coverage over two distinct active sites HC/*1 and HC/*2. Details on the two active sites can be found in Figure S1.7.

Al-sites are completely different, in the sense that they have oxygen coordination of 3 and 5, respectively. As a consequence, the 2-propoxide chemisorption energy on *1 will be much stronger than on-site *2. The Lewis site where cinnamaldehyde adsorbs in all calculated pathways has an oxygen coordination number of 4.

Note that when reaction mechanism are discussed at high coverage, we explicitly mention the 2-proxide that reacts, for example HC/*1, HC/*2 (see Figure S1.7). The chemisorption of 2-propanol on a particular site is followed by the adsorption of cinnamaldehyde either at a free adjacent Al site (dual-site mechanisms LC/*1, HC/*1 and HC/*2; in Figure 6a) or at the same Al site where already the alcohol has been adsorbed (a single site mechanism; LC/*single site; in Figure 6a).

Owing to the significant steric hindrance imposed by the closeness of the bulky cinnamaldehyde and 2-propanol; this step is strongly endergonic by 128 kJ/mol for a single site mechanism (black trace, A→B, Figure 6b). Considering these unfavorable energetics it is unlikely that this reaction path significantly contributes to the overall observed catalytic activity. Avoiding the steric hindrance by placing the bulky aldehyde at an adjacent bare Al site renders this reaction

approximately thermoneutral, i.e. the change in energy is far below ±10 kJ/mol (red trace, A→B, Figure 6b). This is not unexpected, considering that only weak van-der-Waals interactions characterize the adsorption of an aldehyde at the Al site.

Once both reactants have been adsorbed, the reduction of cinnamaldehyde to cinnamyl alcohol can take place through a hydrogen transfer from 2-propanol to the aldehyde (B→C in Figure 6a). For a single site mechanism, this reaction is slightly endergonic by 24 kJ/mol and associated with a minor activation barrier of 36 kJ/mol (black trace, Figure 6b). Thus, this reaction is feasible under reaction conditions provided the two reactants could be placed at the same catalytic site. This is contrasted by the dual-site mechanism where the equivalent hydrogen transfer is strongly endergonic by 70 kJ/mol (red trace, Figure 6b). Accordingly, it is already from a purely thermodynamic perspective unlikely that the reaction can proceed through this path. In the light of these unfavourable energetics and the significant costs associated with estimating activation barriers for the indirect hydrogen transfer between the two adsorbates, no activation barriers were computed.

The hydrogen transfer is followed by the subsequent release of the products (C→D and D→P black trace, Figure 6a). These steps are again unproblematic for a single-site mechanism, i.e. the release of acetone is exergonic by −34 kJ/mol followed by an approximately thermoneutral release of cinnamyl alcohol (red trace, Figure 6b). For a dual-site mechanism, the release reaction is, due to the intermediates being very strongly bound, significantly less favourable. The latter requires 51 kJ/mol to overcome the thermodynamic barrier for the release of acetone while the release of cinnamyl alcohol is again approximately thermoneutral. It is important to note that only a bare surface without any excess 2-propanol adsorbed has been considered.

However, at a large excess of 2-propanol in the solution, the surface may at least partially be covered by this species. To model such a high coverage situation, 2-propanol molecules at Al adsorption sites were placed on the γ-Al_2O_3 (110) model (*1 and *2). This allows for the construction of two high coverage models, HC/*1 and HC/*2. Dependent on the position of the 2-propoxide (see Figure S1.6), a different empty site and thus, reaction mechanism can be operative (see Figure S1.7). Furthermore, having determined, that the single site mechanism is sterically hindered and therefore highly unlikely, we decided only to consider the dual-site path. Comparing the adsorption energies of the initial adsorption of the 2-propanol molecules, we found that the empty HC/*1 site binds, in the presence of a second 2-propanol molecule, the cinnamaldehyde very strongly with a binding energy of −150 kJ/mol (blue trace, Figure 6c). This is opposed to the HC/*2 sites where the adsorption of 2-propyl alcohol is even slightly endergonic by 13 kJ/mol (green trace, Figure 6c). In line with the very strong binding of the initial 2-propanol, we also find the subsequent intermediates B, C and D to bind very strongly (blue trace, Figure 6c) at the HC/*1 site. As a result of this, the MPV reaction is equivalent to the low coverage case blocked by the energetically unfavourable release of the products. This is opposed to the MPV over the HC/*2 site. Here, the slightly endergonic initial reaction is followed by slightly exergonic adsorption of cinnamaldehyde and an equally exergonic hydrogen transfer from 2-propanol to cinnamaldehyde (green trace, A→B and B→C in Figure 6c). The release of the products is finally only slightly endergonic by 7 kJ/mol and 31 kJ/mol for C→D and D→P, respectively (HC/*2, Figure 6c). Overall, the MPV over the HC/*2 pathway displays a much more balanced energy profile which is typically considered as a prerequisite for a highly active catalyst.

2.5. Catalyst selection rules for the HC/*2 pathway

Having established a mechanistic understanding of the MPV over γ-Al_2O_3 it is finally possible to develop a more general understanding of the requirements for highly active materials for the MPV using volcano plots. Volcano plots have previously been used successfully to compare a wide range of catalytic systems ranging from homogeneous catalysts[82,83] to electrocatalysts[84–86] and heterogeneous catalysis.[87] Computational volcano plots fundamentally rely on the detailed knowledge of the reaction mechanism and the fact that the binding energies of the intermediates cannot be varied independently but instead are described by a set of linear equations, the so-called linear free energy scaling relationships (LFESR).[88–90] Suitable LFESRs for the MPV reaction are obtained by computing the binding energies of the intermediates A to D for a large data set (in the present case 15 main group and transition metal oxides) and plotting the binding energies of the descriptor intermediate (x-axis) versus that of the other intermediates (y-axis). The descriptor intermediate is typically chosen such that the best correlation between the data points is obtained. Details on the obtained LFESRs for the MPV reaction can be found in Figure S1.8. When performing such an analysis, the computations are often restricted to only include thermodynamics. This can be justified considering that thermodynamically unfavourable catalysts will not display favourable kinetics. Furthermore, materials with similar binding energies are known to display comparable activation barriers since thermodynamics and kinetics are known to be connected through Brønsted-Evans-Polanyi relationships.[83,91–94]

Following this procedure and using the free energy of intermediate state B (2-propoxide + adsorbed cinnamaldehyde) or ΔG(B) as the reference state, strong scaling relations are found for ΔG(A), and ΔG(C) (Figures S1.8a and S1.8b). On the other hand, only fair scaling between ΔG(D) and ΔG(B) is obtained (Figure S1.8c). These relationships can be expected to hold both for high and low coverage situations since steric interactions have been observed only to affect kinetics but not scaling relations between thermodynamic properties.[83,95]

Based on the LFERs it is now possible to predict the reaction energies of all considered reaction steps for a given descriptor, for example, the binding free energy. By considering only the energetically least favourable step for a given descriptor value, the volcano plot shown in Figure 7 is obtained. This volcano corresponds to a graphical representation of Sabatier's principle,[96] which indicates that an ideal catalyst binds the intermediates neither too strong nor too weak. Such a balanced

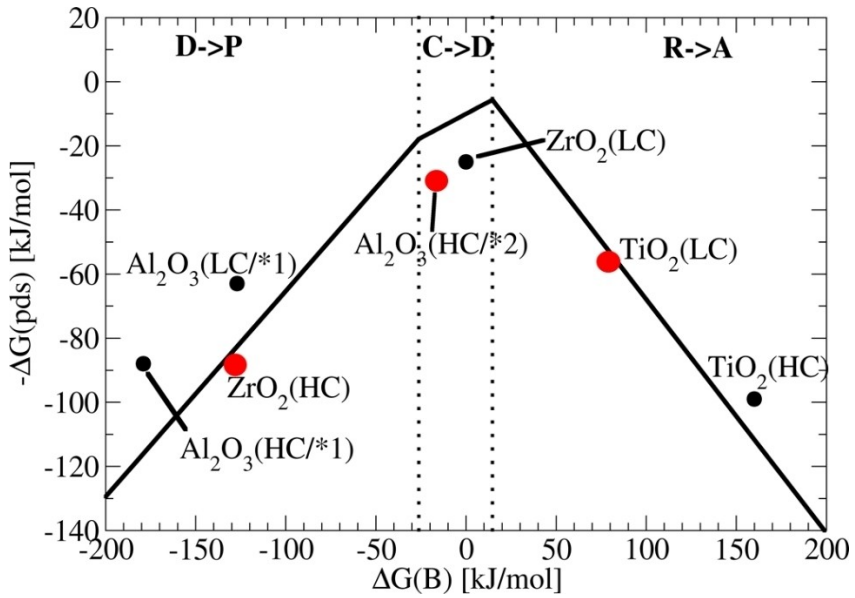

Figure 7. Volcano plot with potential determining steps (pds). Closed red dots are assigned to the thermodynamically most likely catalytic cycle.

catalyst is typically placed at the top of the volcano (Region C→D in Figure 7). Materials which bind the intermediates too strongly and consequently are blocked by the release of the products are found at the left branch of the volcano the so-called strong binding side (Region D→P in Figure 7) and materials which bind too weakly are found at the right slope of the volcano the so-called weak binding side (Region R→A in Figure 7). In the case of the MPV reaction, the strong binding side is determined by the release of cinnamyl alcohol (D→P in Figure 6a) whereas the weak binding side is determined by the adsorption of 2-propanol (R→A in Figure 6a). For the most ideal catalysts placed at the top of the volcano finally, the release of acetone (C→D in Figure 6a) determines the thermodynamic limit. Nevertheless, also the hydrogen exchange reaction (B → C) and the co-adsorption of cinnamaldehyde (A→B) are energetically close to the potential determining step (pds) at the peak of the volcano depicted in Figure S1.7. Despite the overall reaction being exergonic by −12.5 kJ/mol, a slightly endergonic potential determining step (pds) is observed at the top.

To this extent, ZrO_2, TiO_2, and γ-Al_2O_3 have been considered experimentally, with similar conversion and selectivity of 20% for ZrO_2, 70% for TiO_2 and 99% for γ-Al_2O_3 during cinnamaldehyde transfer hydrogenation reaction. The experimental results can be compared using a volcano plot by assuming a low 2-propoxide coverage situation. ZrO_2 is expected to be an excellent catalyst for MPV at low coverage (ZrO_2(LC), Figure 7), however, the adsorption of 2-propoxide at low coverage is also endergonic ($\Delta G(A) > 0$), while a higher 2-propoxide coverage is strongly exergonic ($\Delta G(A) \ll 0$). The latter situation leads to the placement of ZrO_2(HC) at the strong binding site of the volcano in Figure 7, where the co-adsorption of cinnamaldehyde from the high coverage state is still exergonic ($\Delta G(B) < \Delta G(A) \ll 0$). Since the high 2-propoxide coverage situation is thermodynamically more stable, it must also be expected under experimental conditions with a potentially determining step (ΔG(pds)) increased to 88 kJ/mol. In the case of TiO_2, this is placed at the weak binding site and shows (TiO_2(LC), Figure 7). Here, the TiO_2, 2-propoxide formation is endergonic ($\Delta G(A) > 0$) as well as the co-adsorption of cinnamaldehyde from state A ($\Delta G(B) > \Delta G(A) > 0$). From the thermodynamics, it is thus not reasonable to assume an even higher 2-propoxide coverage is likely on the investigated TiO_2(110) surface. However, based on calculations, we can show that at high 2-propoxide coverage, the catalytic activity shifts even to weaker binding sites (TiO_2(HC)) as in Figure 7. Experimentally, we can expect a low coverage of 2-propoxides, which brings the potential determining step (ΔG(pds)) at 56 kJ/mol.

Finally, for γ-Al_2O_3, the three different dual-site pathways are considered above (see also Figure 6), and can also be ranked on the volcano plot. From these three situations, high 2-propoxide coverage Al_2O_3 where the weakly bound 2-propanol reacts (HC/*2) is closest to the top of the volcano plot with a slightly endergonic potential determining step of only 31 kJ/mol (Figure 7). Based on thermodynamics, this situation has also been found to be the most likely pathway on γ-Al_2O_3 clearly shown in Figure 6. Thus, excellent performance can be expected for γ-Al_2O_3. From the volcano plot and the ab initio thermodynamics of 2-propoxide adsorption, the expected activity of the investigated surfaces can be ranked based on the potential determining step, and follows the following trend: γ-Al_2O_3 (31 kJ/mol) > TiO_2 (56 kJ/mol), ZrO_2 (88 kJ/mol). This trend is perfectly in line with the observed activity within the experiments where γ-Al_2O_3 presents the highest conversion, followed by TiO_2 and ZrO_2.

3. Conclusions

In this work, we have demonstrated that microwave heating of γ-Al_2O_3 enhances the selectivity and efficiency of the MPV reduction of aldehydes to alcohols. The reactions proceed without any dopant in the form of transition metals. The reaction has also a broad substrate scope and is compatible with aromatic, unsaturated, and aliphatic aldehydes delivering the corresponding alcohols in excellent yields. Furthermore, the scope is not limited to aldehyde reduction and can be well applied for the synthesis of ethers. Due to the high purity of the reaction mixtures, the product could be isolated by simple filtration and thus minimizing solvent losses during purification. DFT calculations demonstrate the preference of a γ-Al_2O_3 surface dual-site mechanism over the established single site mechanism. Among other catalysts (e.g., ZrO_2 and TiO_2) γ-Al_2O_3 has the highest catalytic activity. With our volcano plot analysis considering various reaction mechanisms on γ-Al_2O_3, we have identified that the dual site and high coverage reaction mechanism on γ-Al_2O_3 results in the highest catalytic activity. We believe that these findings will pave the way for new microwave heated γ-Al_2O_3 catalyzed reactions.

4. Materials and Methods

4.1. MPV reduction

4.1.1. The reduction of aldehydes to alcohols

The reactions were carried out with γ-Al_2O_3 SBA-200 from Sasol. The reactions were heated in a microwave reactor from Biotage (Biotage Initiator+) in sealed microwave vials.

General experimental procedure for the reduction of aldehydes to alcohols – The appropriate aldehyde (0.8 mmol), γ-Al_2O_3 (SBA-200 from Sasol, 100 mg) and 2-propanol (3 ml) was heated in a sealed microwave vial using a Biotage Initiator$^+$. The temperature was set to 180 °C with a hold time of 40 minutes during which a saturation pressure of 1.5×10^6 Pa was reached. After complete consumption of aldehyde, the reaction mixture was filtered and analyzed with an Agilent 7820A GC equipped with a flame ionization detector to determine conversion and selectivity. In most cases the alcohol can be obtained in a pure form directly after filtration and thus no silica gel chromatography is needed.

4.1.2. Thermal treatment of the γ-Al_2O_3

The filtered solid catalyst was washed with 3 ml of 2-propanol and air-dried at room temperature. Next, the catalyst was calcined in a furnace at 400 °C for 5 h under air, and 4% hydrogen diluted in argon (Ar) for 12 h. As such, the calcined material was used for the next round of reactions. The thermal treatment was repeated three times to ensure reproducibility and robustness of the γ-Al_2O_3

4.1.3. Leaching experiments

To probe leaching of γ-Al_2O_3, 100 mg of γ-Al_2O_3 catalyst was suspended in 2-propanol and placed in the microwave for 40 min at 180 °C. After filtration, 0.8 mmol of cinnamaldehyde was added to the filtered solution and placed it back in the microwave for an additional 40 min at 180 °C. No reaction products were found.

4.2. Product analysis

During optimization GC-FID studies were performed on an Agilent 7820A GC (G4350B) with a 7693A auto-injector equipped with an Agilent J&W HP-5, 30 m, 0.32 mm, 0.25 μm GC Column – 19091J-413 column using nitrogen as carrier gas. The concentrations of the analytes were determined by comparison against an internal standard (*n*-dodecane), standardized by calibration against authentic samples of the pure material. Mass yields of the final product were quantified by using calibration curves of standard samples in the gas chromatograph. Mass balances accounting for $>95\%$ of the carbon content were obtained in all experiments. Reactant conversion, and product selectivity were calculated as follows.

$$Conversion\ \% = \left(\frac{moles\ reacted}{moles\ before\ reaction}\right)x100 \quad (1)$$

$$Selectivity\ \% = \left(\frac{moles\ of\ defined\ product}{moles\ of\ reactant\ consumed}\right)x100 \quad (2)$$

4.3. Nuclear Magnetic Resonance (NMR)

The products were analyzed with ^{1}H Nuclear Magnetic Resonance (NMR) (400 MHz), and ^{13}C NMR (101 MHz) spectra acquired on a Varian 400. The chemical shifts for ^{1}H and ^{13}C NMR spectra reported in parts per million (ppm) relative to the residual peak from solvent $CDCl_3$ as the internal standard; ^{1}H NMR at δ 7.26 ppm and ^{13}C NMR at δ 77.16 ppm. All coupling constants (*J*) are reported in Hertz (Hz), and multiplicities are indicated by s (singlet), d (doublet), t (triplet), dd (doublet of doublets) and m (multiplet). Furthermore, high-resolution mass spectrometry (HRMS) was performed on an Agilent 6520 Accurate-Mass Q-TOF equipped with an electrospray interface for new compound identification. NMR and HRMS are presented in supporting section 2.

4.4. Diffuse Reflectance Infrared Fourier Transform (DRIFT) spectroscopy

The adsorbed species over γ-Al_2O_3 were characterized in a high-temperature cell with CaF_2 optical access windows for Diffuse Reflectance Infrared Fourier Transform (DRIFT) Spectroscopy from Harrick Scientific, Pleasantville, NY, USA. The DRIFT cell

was mounted on an infrared spectrometer from Bruker Optics (Tensor 70) with an MCT D316/6-L detector cooled with N_2 adapted with a commercial DRIFT cell (Spectra-Tech.) consisted of four aligned concave polished mirrors mounted on a holder to achieve IR collection of the outgoing signal.

4.4.1. γ-Al_2O_3 pre-treatment

The samples were pressed into tablets and then crushed in a mortar enlarging the powder particles to avoid channelling during the measurement. Subsequently, the powder fraction of the crushed tablets was sieved to a size range of 38 to 75 μm. Then 0.2 g of pre-treated catalyst were placed over KBr bed in the DRIFT reaction cell, a sample pre-treatment to remove any trace of reactants and reaction products from the catalyst was performed for 2 h flowing 50 mL/min of Ar at 150 °C and cooled the sample back to 100 °C. The sample was left for 1 h before the starting of the experiment to reach a stable IR signal.

Prior to DRIFT measurements, the sample was pre-treated in N_2 at 200 °C for 1 h. Followed by 100 mL/min of 99% pyridine or 98% 2,6-lutidine both saturated in N_2 for 1 h. During DRIFT experiments, both of these organic compounds were ice-cooled and bubbled for 30 min at 100 mL/min in N_2 before saturation. The IR spectra were recorded with a resolution of 8 cm^{-1} and 156 co-added scans for 3 h. The reported IR spectra were measured against N_2 used as background and shown baseline-corrected.

4.5. Computational details

To study the MPV reduction, periodic DFT-D calculations are performed with the Vienna Ab Initio Simulation Package (VASP 5.4.4).[97,98] The BEEF-vdW functional was employed to account for van der Waals interactions during the MPV-reduction.[99] The one-electron Kohn-Sham orbitals were expanded in a plane-wave basis set with a kinetic energy cut-off of 550 eV and the core electrons were approximated within the projector augmented wave method (PAW)[100] was used, and for the Brillouin zone sampling different k-point grids were employed depending on the system size (supporting section 1.2, Table S1). A Gaussian smearing[97] of 0.1 eV was applied to improve convergence. Additionally, the convergence criterion for the self-consistent electronic field (SCF) problem is set to 10^{-6} eV for cell optimizations. For γ-Al_2O_3, a periodic 110 surface slab was constructed, the surface is composed of 4 layers of Al_8O_{12} to obtain periodic unit cells terminated with surface OH groups[101–103] shown in supporting section 1.3, Figure S1.2. Transition states are obtained initially with the climbing image nudged elastic band method[104,105] and further refined with the dimer method.[106] Furthermore, the (110) facets of different oxides of the rutile type (TiO_2, SnO_2, GeO_2, HfO_2, IrO_2, MnO_2, RhO_2, RuO_2, ZrO_2) and (110) facets corundum type oxides (Cr_2O_3, Sc_2O_3) and the (100) facets of the rock salt type oxides (CaO, FeO) were taken to construct the linear free energy relations for the reduction of cinnamaldehyde with isopropanol. Four different thermodynamic intermediate states are required to describe the reaction mechanism.

Convergence of transition states and the intermediates' geometries is assumed if the largest force was below 0.05 eV/Å. For the γ-Al_2O_3 model systems, partial Hessian vibrational analysis (PHVA) is employed only for the surface species while keeping the rest of the system fixed. The numerical partial Hessian was calculated by displacements in x, y, and z-directions of ± 0.02 Å, and the vibrational modes were extracted using the normal mode analysis as implemented in the post-processing toolkit TAMKIN.[107] A complete loss in translational and rotational entropy of alcohols and aldehydes was assumed upon chemisorption or adsorption on the γ-Al_2O_3 model (Figure S1.2). The Gibbs free energies are calculated at 180 °C, assuming partial pressure (P_r) for the different reactants. For example, the estimated P for isopropanol ($P_{isopropanol}$) was 4.7×10^7 Pa, and the P for cinnamyl alcohol, cinnamaldehyde, acetone ($P_{cinnamyl\ alcohol} = P_{cinnamaldehyde} = P_{acetone}$) was 0.47×10^6 Pa for 50% conversion, and 0.94×10^6 Pa for 100% conversion.

In the PHVA-procedure, small imaginary modes were replaced by 50 cm^{-1} in the construction of the vibrational partition function.[108] The PHVA was used to obtain zero-point corrections and free energy contributions.[77,78,109] The corrections obtained for γ-Al_2O_3 were used for the other model systems. This approach was approximative but frequently applied in the construction of linear free energy reactions, for example, in electrochemistry during the oxygen evolution reaction (OER).[84,85]

Acknowledgements

Formas (2016-00484) is gratefully acknowledged for funding. H. S., B. D., A. S-A., C. L., K. M.-P. and A. P. would also like to thank Knut and Alice Wallenberg Foundation for support via project 2015.0055. Computational resources and services used for this work were provided by C3SE (Göteborg) and ICHEC (Ireland). H. H. also acknowledge the Competence Centre for Catalysis hosted by Chalmers University of Technology and financially supported by the Swedish Energy Agency and the member companies AB Volvo, ECAPS AB, Johnson Matthey AB, Preem AB, Scania CV AB, Umicore Denmark ApS and Volvo Car Corporation AB. A.S.-A. would like to thank Dr. Dirk Niemeyer from Sasol Limited for the provided γ-Al_2O_3 samples.

Conflict of Interest

The authors declare no conflict of interest.

Keywords: γ-Al_2O_3 · MPV reduction · Microwave-assisted catalysis

[1] E. R. H. Walker, *Chem. Soc. Rev.* **1976**, *5*, 23.
[2] C. F. Lane, *Chem. Rev.* **1976**, *76*, 773–799.
[3] H. C. Brown, S. Krishnamurthy, *Tetrahedron* **1979**, *35*, 567–607.

[4] P. G. Andersson, I. J. Munslow, *Wiley InterScience (Online service), Modern Reduction Methods, Wiley-VCH*, **2008**.
[5] G. H. Posner, *Angew. Chem. Int. Ed. Engl.* **1978**, *17*, 487–496.
[6] V. J. Shiner, D. Whittaker, *J. Am. Chem. Soc.* **1969**, *91*, 394–398.
[7] J. Magano, J. R. Dunetz, *Org. Process Res. Dev.* **2012**, *16*, 1156–1184.
[8] D. Wang, D. Astruc, *Chem. Rev.* **2015**, *115*, 6621–6686.
[9] H. Meerwein, R. Schmidt, *Justus Liebigs Ann. Chem.* **1925**, *444*, 221–238.
[10] W. Ponndorf, *Zeitschrift für Angew. Chemie* **1926**, *39*, 138–143.
[11] A. L. Wilds, in *Org. React.*, John Wiley & Sons, Inc., Hoboken, NJ, USA, **2011**, pp. 178–223.
[12] G. Brieger, T. J. Nestrick, *Chem. Rev.* **1974**, *74*, 567–580.
[13] G. I. Nikonov, *ACS Catal.* **2017**, *7*, 7257–7266.
[14] P. Nandi, W. Tang, A. Okrut, X. Kong, S.-J. Hwang, M. Neurock, A. Katz, *Proc. Mont. Acad. Sci.* **2013**, *110*, 2484–2489.
[15] G. H. Posner, D. Z. Rogers, *J. Am. Chem. Soc.* **1977**, *99*, 8208–8214.
[16] G. H. Posner, A. W. Runquist, M. J. Chapdelaine, *J. Org. Chem.* **1977**, *42*, 1202–1208.
[17] C. J. Clarke, W.-C. Tu, O. Levers, A. Bröhl, J. P. Hallett, *Chem. Rev.* **2018**, *118*, 747–800.
[18] R. A. Sheldon, *Green Chem.* **2007**, *9*, 1273.
[19] G. Chuah, S. Jaenicke, Y. Zhu, S. Liu, *Curr. Org. Chem.* **2006**, *10*, 1639–1654.
[20] S. Conrad, R. Verel, C. Hammond, P. Wolf, F. Göltl, I. Hermans, *ChemCatChem* **2015**, *7*, 3270–3278.
[21] M. Koehle, R. F. Lobo, *Catal. Sci. Technol.* **2016**, *6*, 3018–3026.
[22] H. Y. Luo, D. F. Consoli, W. R. Gunther, Y. Román-Leshkov, *J. Catal.* **2014**, *320*, 198–207.
[23] M. M. Antunes, S. Lima, P. Neves, A. L. Magalhães, E. Fazio, A. Fernandes, F. Neri, C. M. Silva, S. M. Rocha, M. F. Ribeiro, M. Pillinger, A. Urakawa, A. A. Valente, *J. Catal.* **2015**, *329*, 522–537.
[24] A. Corma, M. E. Domine, L. Nemeth, S. Valencia, *J. Am. Chem. Soc.* **2002**, *124*, 3194–3195.
[25] M. Moliner, Y. Román-Leshkov, M. E. Davis, *Proc. Natl. Acad. Sci. USA* **2010**, *107*, 6164–8.
[26] M. M. Antunes, S. Lima, P. Neves, A. L. Magalhães, E. Fazio, F. Neri, M. T. Pereira, A. F. Silva, C. M. Silva, S. M. Rocha, M. Pillinger, A. Urakawa, A. A. Valente, *Appl. Catal. B* **2016**, *182*, 485–503.
[27] P. S. Kumbhar, J. Sanchez-Valente, J. Lopez, F. Figueras, *Chem. Commun.* **1998**, *0*, 535–536.
[28] C. Jiménez-Sanchidrián, J. R. Ruiz, *Appl. Catal. A* **2014**, *469*, 367–372.
[29] A. Segawa, K. Taniya, Y. Ichihashi, S. Nishiyama, N. Yoshida, M. Okamoto, *Ind. Eng. Chem. Res.* **2018**, *57*, 70–78.
[30] B. Zhang, F. Xie, J. Yuan, L. Wang, B. Deng, *Catal. Commun.* **2017**, *92*, 46–50.
[31] M. Fukui, A. Tanaka, K. Hashimoto, H. Kominami, *Chem. Commun.* **2017**, *53*, 4215–4218.
[32] Y. Zhu, S. Liu, S. Jaenicke, G. Chuah, *Catal. Today* **2004**, *97*, 249–255.
[33] T. M. Jyothi, T. Raja, K. Sreekumar, M. B. Talawar, B. S. Rao, *J. Mol. Catal. A* **2000**, *157*, 193–198.
[34] C. R. Graves, E. Joseph Campbell, S. B. T. Nguyen, *Tetrahedron: Asymmetry* **2005**, *16*, 3460–3468.
[35] J. Hidalgo-Carrillo, A. Parejas, M. Cuesta-Rioboo, A. Marinas, F. Urbano, J. Hidalgo-Carrillo, A. Parejas, M. J. Cuesta-Rioboo, A. Marinas, F. J. Urbano, *Catalysts* **2018**, *8*, 539.
[36] V. A. Ivanov, J. Bachelier, F. Audry, J. C. Lavalley, *J. Mol. Catal.* **1994**, *91*, 45–59.
[37] P. J. Larson, J. L. Cheney, A. D. French, D. M. Klein, B. J. Wylie, A. F. Cozzolino, *Inorg. Chem.* **2018**, *57*, 6825–6832.
[38] A. Corma, M. E. Domine, S. Valencia, *J. Catal.* **2003**, *215*, 294–304.
[39] B. Basu, S. Paul, *J. Catal.* **2013**, *2013*, 1–20.
[40] S. Fukuzawa, N. Nakano, T. Saitoh, *Eur. J. Org. Chem.* **2004**, *2004*, 2863–2867.
[41] J. F. Miñambres, M. A. Aramendía, A. Marinas, J. M. Marinas, F. J. Urbano, *J. Mol. Catal. A* **2011**, *338*, 121–129.
[42] C. Li, Y. Chen, S. Zhang, S. Xu, J. Zhou, F. Wang, M. Wei, D. G. Evans, X. Duan, *Chem. Mater.* **2013**, *25*, 3888–3896.
[43] C.-H. Hao, X.-N. Guo, Y.-T. Pan, S. Chen, Z.-F. Jiao, H. Yang, X.-Y. Guo, *J. Am. Chem. Soc.* **2016**, *138*, 9361–9364.
[44] J. M. Hidalgo, C. Jiménez-Sanchidrián, J. R. Ruiz, *Appl. Catal. A* **2014**, *470*, 311–317.
[45] T.-W. Kim, J.-W. Kim, S.-Y. Kim, H.-J. Chae, J.-R. Kim, S.-Y. Jeong, C.-U. Kim, *Chem. Eng. J.* **2015**, *278*, 217–223.
[46] Y. Zhu, G. Chuah, S. Jaenicke, *J. Catal.* **2004**, *227*, 1–10.
[47] V. L. Sushkevich, I. I. Ivanova, S. Tolborg, E. Taarning, *J. Catal.* **2014**, *316*, 121–129.
[48] H. J. Kitchen, S. R. Vallance, J. L. Kennedy, N. Tapia-Ruiz, L. Carassiti, A. Harrison, A. G. Whittaker, T. D. Drysdale, S. W. Kingman, D. H. Gregory, *Chem. Rev.* **2014**, *114*, 1170–1206.
[49] P. Lidström, J. Tierney, B. Wathey, J. Westman, *Tetrahedron* **2001**, *57*, 9225–9283.
[50] M. M. Mojtahedi, A. Sharifi, F. Mohsenzadeh, M. R. Saidi, *Synth. Commun.* **2000**, *30*, 69–72.
[51] B. Touaux, F. Texier-Boullet, J. Hamelin, *Heteroat. Chem.* **1998**, *9*, 351–354.
[52] D. Villemin, B. Martin, *Synth. Commun.* **1998**, *28*, 3201–3208.
[53] P. S. Kwon, Y. M. Kim, C. J. Kang, T. W. Kwon, S. K. Chung, Y. T. Chang, *Synth. Commun.* **1997**, *27*, 4091–4100.
[54] R. S. Varma, D. Kumar, P. J. Liesen, *J. Chem. Soc. Perkin Trans. 1* **1998**, 4093–4096.
[55] P. K. Pradhan, P. Jaisankar, B. Pal, S. Dey, V. S. Giri, *Synth. Commun.* **2004**, *34*, 2863–2872.
[56] R. Cohen, C. R. Graves, S. B. T. Nguyen, J. M. L. Martin, M. A. Ratner, *J. Am. Chem. Soc.* **2004**, *126*, 14796–14803.
[57] J. F. DeWilde, H. Chiang, D. A. Hickman, C. R. Ho, A. Bhan, *ACS Catal.* **2013**, *3*, 798–807.
[58] K. Yuan, T. Song, D. Wang, X. Zhang, X. Gao, Y. Zou, H. Dong, Z. Tang, W. Hu, *Angew. Chem. Int. Ed.* **2018**, *57*, 5708–5713; *Angew. Chem.* **2018**, *130*, 5810–5815.
[59] R. L. Burwell, W. R. Patterson, *J. Am. Chem. Soc.* **1971**, *93*, 833–838.
[60] A. De La Hoz, Á. Díaz-Ortiz, A. Moreno, *Chem. Soc. Rev.* **2005**, *34*, 164–178.
[61] L. Ricciardi, W. Verboom, J.-P. Lange, J. Huskens, *ChemSusChem* **2020**, cssc.202000966.
[62] X. Zhang, D. O. Hayward, D. M. P. Mingos, *Chem. Commun.* **1999**, 975–976.
[63] A. Ramirez, J. L. Hueso, M. Abian, M. U. Alzueta, R. Mallada, J. Santamaria, *Sci. Adv.* **2019**, *5*, eaau9000.
[64] G. D. Yadav, P. M. Bisht, *Catal. Commun.* **2004**, *5*, 259–263.
[65] S. Marx, B. Ndaba, *Biofuels Bioprod. Biorefin.* **2019**, 1–8.
[66] D. Zhao, Y. Wang, F. Delbecq, C. Len, *Mol. Catal.* **2019**, *475*, 110456.
[67] W. Ouyang, D. Zhao, Y. Wang, A. M. Balu, C. Len, R. Luque, *ACS Sustainable Chem. Eng.* **2018**, *6*, 6746–6752.
[68] Y. Wang, D. Zhao, D. Rodríguez-Padrón, C. Len, *Catalysts* **2019**, *9*, 796.
[69] Y. Wang, P. Prinsen, K. S. Triantafyllidis, S. A. Karakoulia, A. Yepez, C. Len, R. Luque, *ChemCatChem* **2018**, *10*, 3459–3468.
[70] R. López-Asensio, J. A. Cecilia, C. P. Jiménez-Gómez, C. García-Sancho, R. Moreno-Tost, P. Maireles-Torres, *Appl. Catal. A* **2018**, *556*, 1–9.
[71] L. Samain, A. Jaworski, M. Edén, D. M. Ladd, D.-K. Seo, F. Javier Garcia-Garcia, U. Häussermann, *J. Solid State Chem.* **2014**, *217*, 1–8.
[72] M. I. Zaki, M. A. Hasan, F. A. Al-Sagheer, L. Pasupulety, *Colloids Surf. A* **2001**, *190*, 261–274.
[73] A. Takagaki, J. C. Jung, S. Hayashi, *RSC Adv.* **2014**, *4*, 43785–43791.
[74] L. Oliviero, A. Vimont, J.-C. Lavalley, F. Romero Sarria, M. Gaillard, F. Maugé, *Phys. Chem. Chem. Phys.* **2005**, *7*, 1861–1869.
[75] A. Corma, C. Rodellas, V. Fornes, *J. Catal.* **1984**, *88*, 374–381.
[76] O. Björneholm, M. H. Hansen, A. Hodgson, L. M. Liu, D. T. Limmer, A. Michaelides, P. Pedevilla, J. Rossmeisl, H. Shen, G. Tocci, E. Tyrode, M. M. Walz, J. Werner, H. Bluhm, *Chem. Rev.* **2016**, *116*, 7698–7726.
[77] M. Vandichel, J. Hajek, A. Ghysels, A. De Vos, M. Waroquier, V. Van Speybroeck, *CrystEngComm* **2016**, *18*, 7056–7069.
[78] J. Hajek, M. Vandichel, B. Van De Voorde, B. Bueken, D. De Vos, M. Waroquier, V. Van Speybroeck, *J. Catal.* **2015**, *331*, 1–12.
[79] F. Gonell, M. Boronat, A. Corma, *Catal. Sci. Technol.* **2017**, *7*, 2865–2873.
[80] S. Rojas-Buzo, P. García-García, A. Corma, *ChemSusChem* **2018**, *11*, 432–438.
[81] M. Boronat, A. Corma, M. Renz, *J. Phys. Chem. B* **2006**, *110*, 21168–21174.
[82] M. Busch, M. D. Wodrich, C. Corminboeuf, *ACS Catal.* **2017**, *7*, 5643–5653.
[83] M. D. Wodrich, M. Busch, C. Corminboeuf, *Chem. Sci.* **2016**, *7*, 5723–5735.
[84] I. C. Man, H.-Y. Su, F. Calle-Vallejo, H. A. Hansen, J. I. Martínez, N. G. Inoglu, J. Kitchin, T. F. Jaramillo, J. K. Nørskov, J. Rossmeisl, *ChemCatChem* **2011**, *3*, 1159–1165.
[85] M. Busch, N. B. Halck, U. I. Kramm, S. Siahrostami, P. Krtil, J. Rossmeisl, *Nano Energy* **2016**, *29*, 126–135.
[86] J. G. Howalt, T. Bligaard, J. Rossmeisl, T. Vegge, *Phys. Chem. Chem. Phys.* **2013**, *15*, 7785.
[87] J. K. Nørskov, T. Bligaard, J. Rossmeisl, C. H. Christensen, *Nat. Chem.* **2009**, *1*, 37–46.

[88] F. Calle-Vallejo, J. I. Martínez, J. M. García-Lastra, J. Rossmeisl, M. T. M. Koper, *Phys. Rev. Lett.* **2012**, *108*, 116103.
[89] F. Abild-Pedersen, J. Greeley, F. Studt, J. Rossmeisl, T. R. Munter, P. G. Moses, E. Skúlason, T. Bligaard, J. K. Nørskov, *Phys. Rev. Lett.* **2007**, *99*, 016105.
[90] M. Busch, M. D. Wodrich, C. Corminboeuf, *Chem. Sci.* **2015**, *6*, 6754–6761.
[91] J. K. Nørskov, T. Bligaard, A. Logadottir, S. Bahn, L. B. Hansen, M. Bollinger, H. Bengaard, B. Hammer, Z. Sljivancanin, M. Mavrikakis, Y. Xu, S. Dahl, C. J. H. Jacobsen, *J. Catal.* **2002**, *209*, 275–278.
[92] A. Vojvodic, F. Calle-Vallejo, W. Guo, S. Wang, A. Toftelund, F. Studt, J. I. Martínez, J. Shen, I. C. Man, J. Rossmeisl, T. Bligaard, J. K. Nrskov, F. Abild-Pedersen, *J. Chem. Phys.* **2011**, *134*, 244509.
[93] *Proc. R. Soc. London Ser. A* **1936**, *154*, 414–429.
[94] M. G. Evans, M. Polanyi, *Trans. Faraday Soc.* **1938**, *34*, 11–24.
[95] M. D. Wodrich, B. Sawatlon, M. Busch, C. Corminboeuf, *ChemCatChem* **2018**, *10*, 1586–1591.
[96] P. Sabatier, *Ber. Dtsch. Chem. Ges.* **1911**, *44*, 1984–2001.
[97] G. Kresse, J. Furthmüller, *Comput. Mater. Sci.* **1996**, *6*, 15–50.
[98] G. Kresse, J. Furthmüller, *Phys. Rev. B* **1996**, *54*, 11169–11186.
[99] J. Wellendorff, K. T. Lundgaard, A. Møgelhøj, V. Petzold, D. D. Landis, J. K. Nørskov, T. Bligaard, K. W. Jacobsen, *Phys. Rev. B* **2012**, *85*, 235149.
[100] P. E. Blöchl, *Phys. Rev. B* **1994**, *50*, 17953–17979.
[101] R. Wischert, P. Florian, C. Copéret, D. Massiot, P. Sautet, *J. Phys. Chem. C* **2014**, *118*, 15292–15299.
[102] S. Klacar, H. Gronbeck, *Catal. Sci. Technol.* **2013**, *3*, 183–190.
[103] R. Wischert, C. Copéret, F. Delbecq, P. Sautet, *Angew. Chem. Int. Ed.* **2011**, *50*, 3202–3205; *Angew. Chem.* **2011**, *123*, 3260–3263.
[104] G. Mills, H. Jónsson, G. K. Schenter, *Surf. Sci.* **1995**, *324*, 305–337.
[105] G. Henkelman, H. Jónsson, *J. Chem. Phys.* **2000**, *113*, 9978.
[106] G. Henkelman, H. Jónsson, *J. Chem. Phys.* **1999**, *111*, 7010.
[107] A. Ghysels, T. Verstraelen, K. Hemelsoet, M. Waroquier, V. Van Speybroeck, *J. Chem. Inf. Model.* **2010**, *50*, 1736–1750.
[108] B. A. De Moor, A. Ghysels, M.-F. Reyniers, V. Van Speybroeck, M. Waroquier, G. B. Marin, *J. Chem. Theory Comput.* **2011**, *7*, 1090–1101.
[109] M. Vandichel, J. Hajek, F. Vermoortele, M. Waroquier, D. E. De Vos, V. Van Speybroeck, *CrystEngComm* **2015**, *17*, 395–406.

Manuscript received: August 5, 2020
Revised manuscript received: August 31, 2020
Version of record online: October 23, 2020